Cardiac Strains from DENSE MRI: Evaluation of SNR Requirements and Strain Error using a Computational Phantom

Ilya A. Verzhbinsky, Luigi E. Perotti, Kévin Moulin, Tyler E Cork, Michael Loecher, Daniel B. Ennis

Synopsis (100 words)

Displacement Encoding with Stimulated Echoes (DENSE) MRI encodes high-resolution cardiac tissue displacements into the phase of the complex MR signal. However, due to the inherent difficulty of obtaining ground truth strain measurements in the beating heart, it remains unclear how image SNR impacts the bias and range of error for computed cardiac strains. In this work, we present a computational deforming heart-like phantom to evaluate cardiac strains computed using a widely available, open-source DENSE Image Analysis Tool. We show that a strain error range within 0.05 and near-zero median error bias can be achieved with SNR>20.

Body (750 words)

Introduction:

Displacement Encoding with Stimulated Echoes (DENSE) MRI encodes tissue displacements into the phase of the complex MR signal. Due to its high spatial and temporal resolution, DENSE MRI is effective for measuring regional cardiac strains in the clinic[1,2] and in preclinical modeling studies evaluating myocardial stiffness[3] and kinematics[4].

Different encoding strategies have been proposed to minimize phase variance and maximize signal-to-noise ratio (SNR) in the acquired DENSE images. Although these encoding strategies have been validated using gel phantoms[5], it remains unclear how image SNR specifically impacts measured cardiac strains along the circumferential (E_{cc}), radial (E_{rr}), longitudinal (E_{ll}) and cardiomyocyte aggregate (i.e. “fiber”) (E_{ff}) directions. This is due to the inherent difficulty of obtaining ground truth strain measurements in the beating heart.

The objectives of this work were: 1) to quantify the accuracy and precision of cardiac strains computed using the most widely available, open-source DENSE Image Analysis Tool[6]; and 2) to quantify how image SNR propagates through the DENSE encoding and processing pipeline to impact the bias and range of computed E_{cc}, E_{rr}, E_{ll} and E_{ff}.

Methods:

We use an axial-symmetric deforming heart-like computational phantom with time-resolved deformation defined by three analytical functions for radial, circumferential, and longitudinal motion. The target ground-truth peak systolic strains were calibrated based on strain reports from *in vivo* DENSE studies[8] (Fig. 1).

The analytic phantom deformation field was subdivided into a grid of 2.5x2.5x8mm voxels at two slice locations, spaced 8mm from each other. To account for intravoxel dephasing and partial

volume effects, Eulerian tissue displacements were sampled at 12 points within each voxel, and averaged to generate a bulk displacement vector per voxel. The corresponding phase was computed by scaling the bulk displacement components according to an encoding strength of 0.08 cycles/mm. The signal magnitude was computed as the average magnitude across all intravoxel sampling points, assuming a signal of 0 for air and 1 for myocardium (Fig. 2A).

DENSE imaging typically employs a balanced 4-point encoding scheme. To properly account for noise, the phantom displacements were transformed into the corresponding balanced 4-point phase maps according to the encoding matrix outlined in Zhong *et al.*[5] Complex valued noise was added to the four phase maps for a range of ten different SNRs (2, 5, 10, 20, 30, 40, 60, 80, 160, 320). Finally, the resulting noise-injected complex images were encoded back into phase along x, y, and z (Fig. 2B-D). Each SNR simulation was repeated five times for strain analysis.

Lagrangian phantom displacements in x, y and z were extracted from the signal phase using the DENSE Image Analysis Tool[6]. Using a mesh-free interpolation scheme[7], myocardial E_{cc}, E_{rr}, E_{ll}, and E_{ff} between the two simulated slice locations were computed at 200 points and across the range of DENSE SNRs. Pointwise strain difference, defined as ground truth strain minus computed DENSE strain, was measured at all 200 sampled points for each SNR repetition and quantified through the heart wall. We set a standard of near-zero strain bias and a strain error range within 0.05.

Results:

E_{ff}, E_{cc}, E_{ll}, and mid-wall E_{rr} exhibit near-zero median strain bias across SNRs (Fig. 4). Epicardial and endocardial E_{rr} show a strain bias of -0.08 and +0.01 at the endocardium and epicardium, respectively.

The 95%-confidence interval (95%-CI) of strain differences for E_{ff}, E_{cc}, $E_{ll,}$ and mid-wall E_{rr} tightens within a range of 0.05 for SNR>20 (Fig 4D). 95%-CI of epi- and endocardial E_{rr} error does not converge within 0.05.

Discussion:

At SNR = 320, the median and range of strain error is near-zero for E_{ff}, E_{cc}, and E_{ll}, indicating the DENSE Analysis Tool accurately and precisely characterizes these cardiac strains (Fig. 3). E_{rr} exhibited pronounced computed strain bias and a broad 95%-CI even at SNR = 320 (Fig. 4). It remains to be investigated if E_{rr} is therefore more susceptible to voxel size and/or the numerical method used to differentiate the DENSE displacement field.

This study demonstrates that the precision of computed strains, and not the bias, is primarily impacted by image SNR. The measured impact of SNR on strain precision can help guide analysis of longitudinal clinical studies of DENSE MRI strains.

Conclusion:

We find that E_{ff}, E_{cc}, E_{ll} and mid-wall E_{rr} are computed with near-zero median bias and within a strain error range of 0.05 for SNR>20. The flexibility of our validation pipeline allows for future

assessment of the impact that other imaging parameters (e.g., resolution, encoding strength, number of encoding directions) have on measured cardiac strains. These simulations can provide *a priori* estimates of required protocol parameters to achieve a target strain sensitivity in clinical studies.

References (750 words)

1 - Aletras AH, Tilak GS, Hsu LY, Arai AE. Heterogeneity of Intramural Function in Hypertrophic CardiomyopathyClinical Perspective: Mechanistic Insights From MRI Late Gadolinium Enhancement and High-Resolution Displacement Encoding With Stimulated Echoes Strain Maps. Circulation: Cardiovascular Imaging. 2011 Jul 1;4(4):425-34.

2 - Bilchick KC, Kuruvilla S, Hamirani YS, Ramachandran R, Clarke SA, Parker KM, Stukenborg GJ, Mason P, Ferguson JD, Moorman JR, Malhotra R. Impact of mechanical activation, scar, and electrical timing on cardiac resynchronization therapy response and clinical outcomes. Journal of the American College of Cardiology. 2014 Apr 29;63(16):1657-66.

3 - Perotti LE, Ponnaluri AV, Krishnamoorthi S, Balzani D, Ennis DB, Klug WS. Method for the unique identification of hyperelastic material properties using full-field measures. Application to the passive myocardium material response. International journal for numerical methods in biomedical engineering. 2017 Nov;33(11):e2866.

4 - Perotti LE, Magrath P, Verzhbinsky IA, Aliotta E, Moulin K, Ennis DB. Microstructurally Anchored Cardiac Kinematics by Combining In Vivo DENSE MRI and cDTI. In International Conference on Functional Imaging and Modeling of the Heart 2017 Jun 11 (pp. 381-391). Springer, Cham.

5 - Zhong X, Helm PA, Epstein FH. Balanced multipoint displacement encoding for DENSE MRI. Magnetic Resonance in Medicine: An Official Journal of the International Society for Magnetic Resonance in Medicine. 2009 Apr;61(4):981-8.

6 - Spottiswoode BS, Zhong X, Hess AT, Kramer CM, Meintjes EM, Mayosi BM, Epstein FH. Tracking myocardial motion from cine DENSE images using spatiotemporal phase unwrapping and temporal fitting. IEEE transactions on medical imaging. 2007 Jan;26(1):15-30.
Code available at: https://github.com/denseanalysis/denseanalysis

7 - Arroyo M, Ortiz M. Local maximum-entropy approximation schemes: a seamless bridge between finite elements and meshfree methods. International journal for numerical methods in engineering. 2006 Mar 26;65(13):2167-202.

8 - Zhong X, Spottiswoode BS, Meyer CH, Kramer CM, Epstein FH. Imaging three-dimensional myocardial mechanics using navigator-gated volumetric spiral cine DENSE MRI. Magnetic resonance in medicine. 2010 Oct;64(4):1089-97.

9 - Ennis DB, Nguyen TC, Riboh JC, Wigström L, Harrington KB, Daughters GT, Ingels NB, Miller DC. Myofiber angle distributions in the ovine left ventricle do not conform to computationally optimized predictions. Journal of biomechanics. 2008 Nov 14;41(15):3219-24.

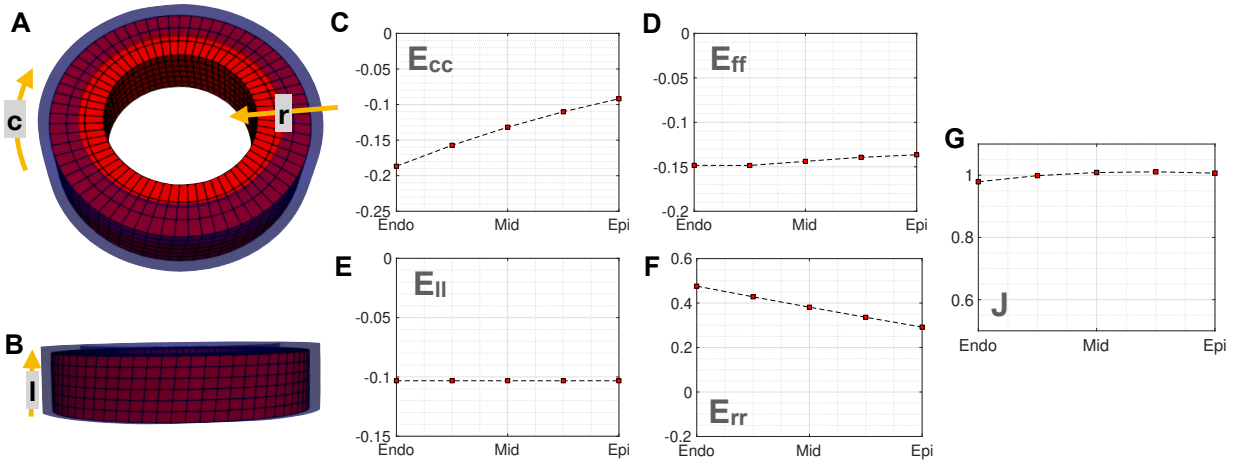

Fig 1. Strain results from the computational deforming phantom. A) Axial and B) longitudinal views of the phantom at beginning (blue) and end (red) systole. Circumferential (c), radial (r) and longitudinal (l) directions are also shown. Cardiomyocyte (f) directions were prescribed in the phantom according to a rule-based approach calibrated on histological data[9]. Transmural strain results from epicardium to endocardium for C) E_{cc}, D) E_{ff}, E) E_{ll}, and F) E_{rr}. G) Transmural Jacobian results. The jacobian (det(**F**)) describes the incompressibility of the myocardium, 1 being perfectly incompressible.

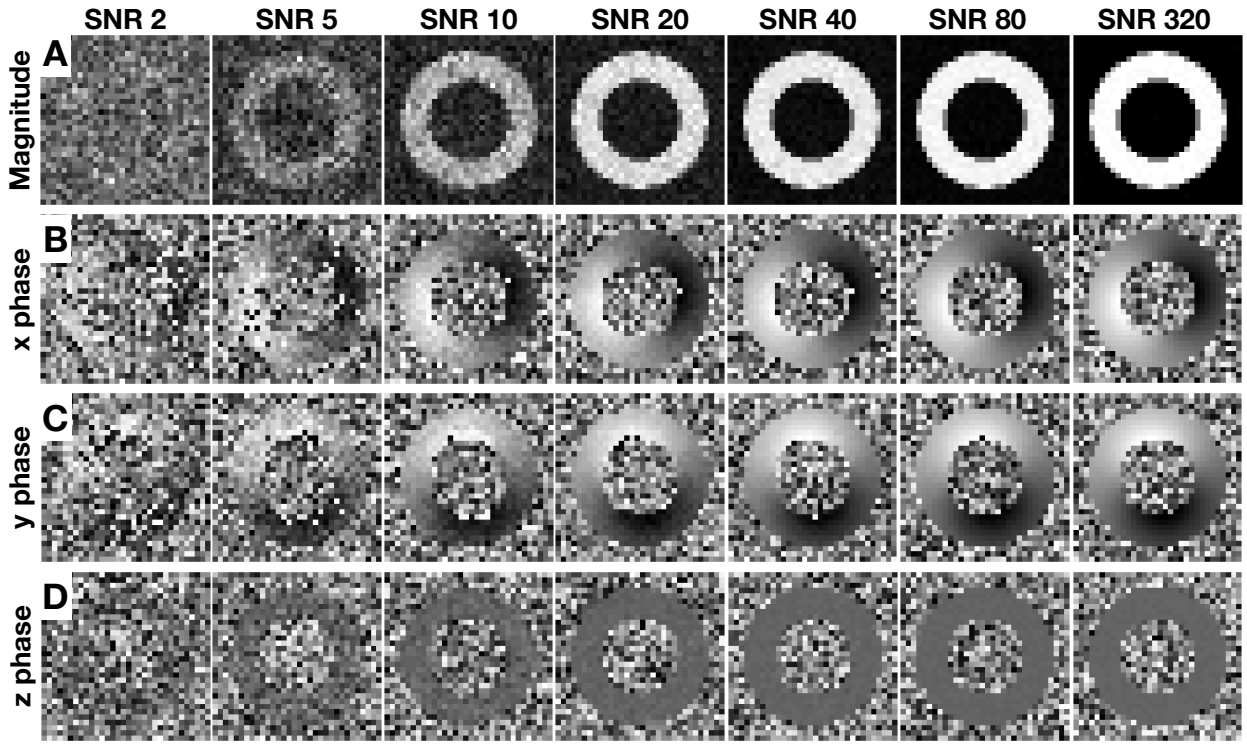

Fig 2. Simulated DENSE magnitude and phase images for a range of SNRs. Results for A) magnitude data, B) x-phase data, C) y-phase data, and D) z-phase data are shown. These data show a single repetition for each SNR, but simulations were repeated five times for each SNR.

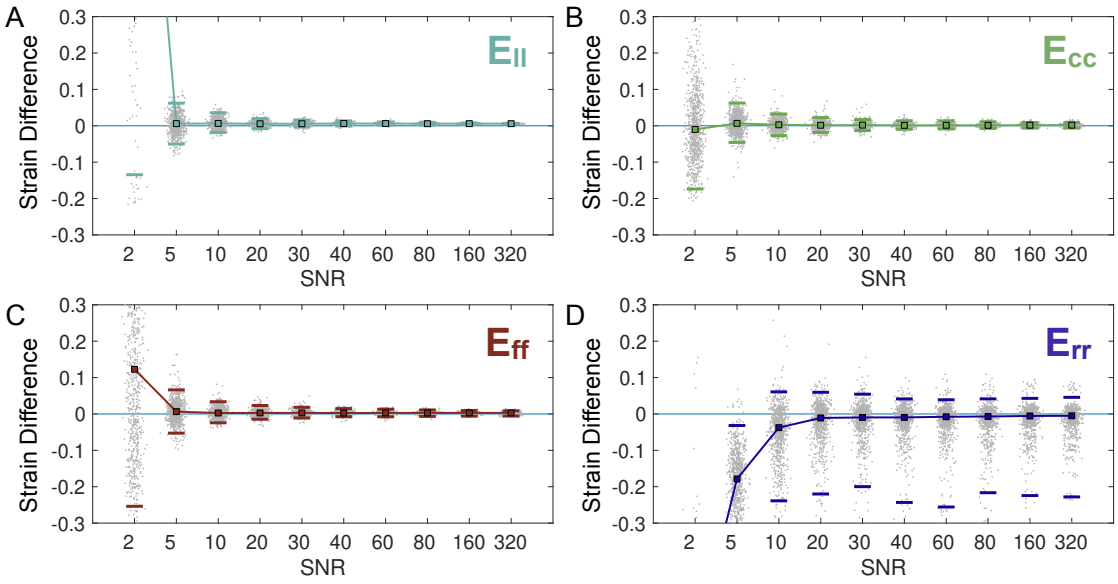

Fig 3. Pointwise strain difference results as a function of image SNR for A) E_{ll}, B) E_{cc}, C) E_{ff}, and D) E_{rr}. Strain difference was computed as ground-truth strain minus DENSE computed strain at each location. Squares represent median difference while horizontal ticks represent 95%-CI across five SNR repetitions.

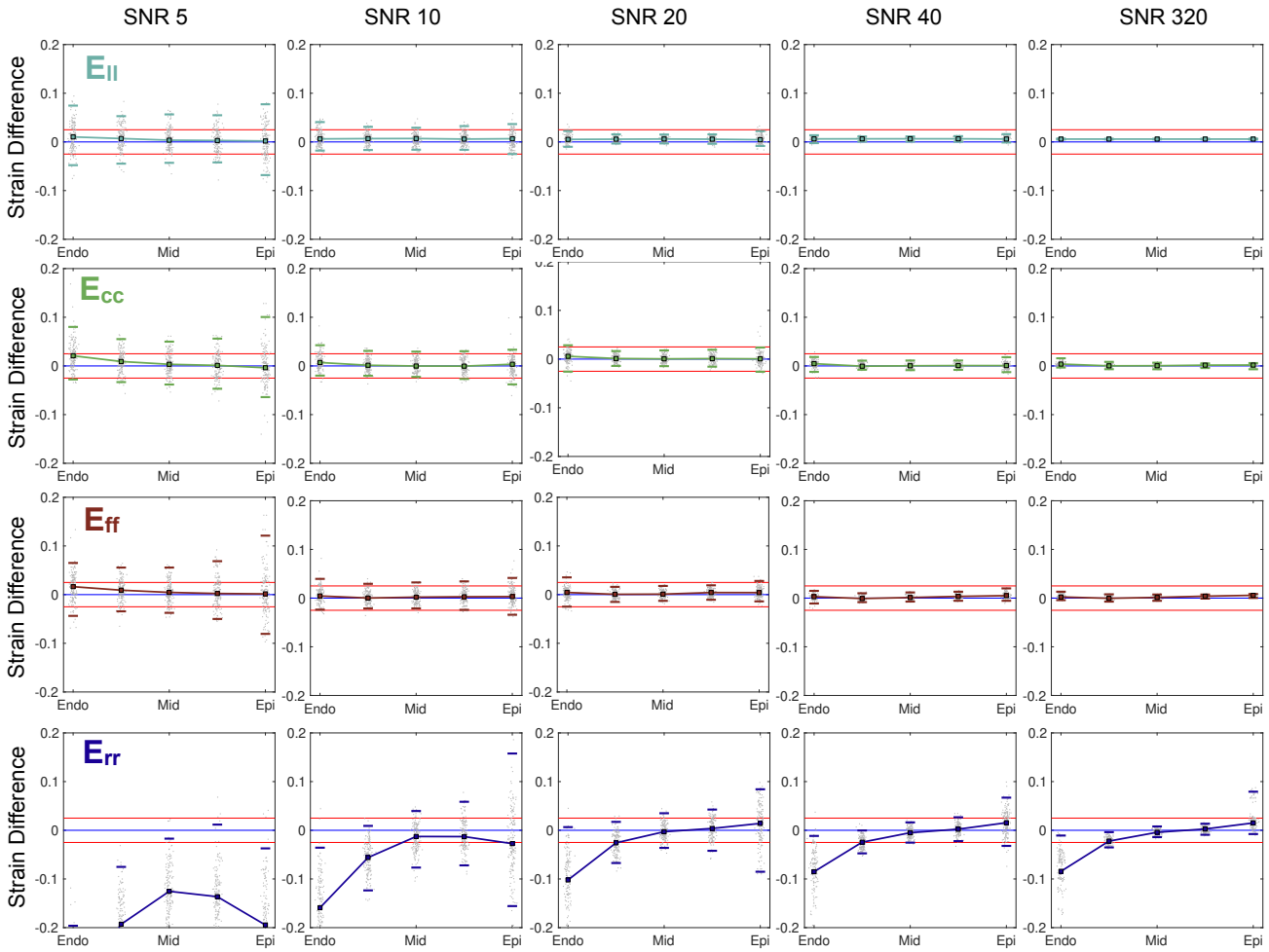

Fig 4. Strain Difference vs. Wall Depth computed at five equidistant transmural points for A) E_{ll}, B) E_{cc}, C) E_{ff}, and D) E_{rr}. Squares represent medians and horizontal ticks represent 95% CI for strain difference values computed across five repetitions for each SNR. Horizonal lines represent 0 strain difference (blue) and 95% CI (red) of +0.025 to -0.025, which is used as one metric of acceptable strain variance.